



## DETERMINATION OF THE NATURE OF ACID SITES IN B-MCM-41 AND Al-MCM-41

Lamia BRAHMI,<sup>a,b,\*</sup> Ali-Dahmane TEWFIK,<sup>c,d,e</sup> Rachida HAMACHA<sup>c</sup> and Salih HACINI<sup>a</sup>

<sup>a</sup> Fine Chemistry Laboratory L.C.F., University of Oran I Ahmed Ben Bella, BP 1524 El-Mnaouer, 31000 Oran, Algeria

<sup>b</sup> Department of Chemistry, Faculty of Science, University Abou Beker Belkaid Tlemcen, BP 119, 13000 Tlemcen, Algeria

<sup>c</sup> Materials Chemistry Laboratory (L.C.M.), Ahmed Ben Bella University of Oran, BP 1524, El-Mnaouer, 31000 Oran, Algeria

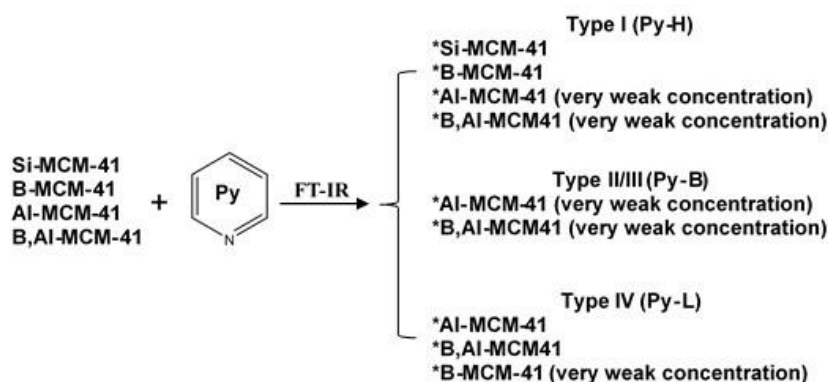
<sup>d</sup> Laboratory of Organic Electrolytes and Polyelectrolytes Application (LAEPO), University Abou Beker Belkaid Tlemcen, BP119, 13000 Tlemcen, Algeria

<sup>e</sup> Tlemcen School of Applied Sciences (ESSA-Tlemcen), BP 165, 13000 Bel Horizon, Tlemcen, Algeria

Received November 25, 2023

Mesoporous purely siliceous MCM-41, B-MCM-41, Al-MCM-41 and B,Al-MCM-41 molecular sieves have been synthesized by the direct hydrothermal method. Colloidal silica, boric acid and sodium aluminate have been used as sources of silica, boron and aluminum respectively. To evaluate the structural and textural parameters of the mesoporous materials, the as-synthesized and calcined samples were characterized by X-ray diffraction, N<sub>2</sub> physisorption and Scanning Electron Microscopy combined with an Energy Dispersive X-ray spectroscopy.

The nature and concentration of the acid sites of the various samples were evaluated by spectroscopic analysis using in situ pyridine adsorption/desorption FT-IR spectroscopy. The structural and textural analyzes confirmed the incorporation of boron and aluminum atoms in MCM-41 framework. The spectroscopic analysis allowed us to develop a model which describes the nature of the acid sites of our materials.



### INTRODUCTION

Since 1992, researchers have been focusing not only on zeolite studies but also on mesoporous materials. Specifically, they have been interested in controlling their texture, the synthesis mechanism in order to gain a deeper comprehension of their

surface state and its potential modifications. This made it possible to better control the application of mesoporous solids as catalyst support<sup>1–4</sup> or adsorbent.<sup>5,6</sup>

The purely siliceous mesoporous MCM-41 material (Si-MCM-41) belongs to the M41S family,<sup>7,8</sup> it is characterized by the presence of

\* Corresponding author: brahmilam@gmail.com

ordered pores with controlled and adjustable size (from 20 to 100 Å), which develops high surface areas that can reach 1500 m<sup>2</sup>/g and large pore volume of the order of 1.2 cm<sup>3</sup>/g. This material has a neutral framework, which restricts its utilization as a catalyst; the substitution of silicon atoms by heteroatoms becomes obvious. The incorporation of heteroatoms such as aluminium or boron creates negative or positive charges in the MCM-41 framework thus creating Brønsted and Lewis acid sites.

Al-containing MCM-41 materials have been extensively studied.<sup>9</sup> These studies showed that the choice of the source of sodium aluminate incorporates the highest quantity of aluminum atoms into the structure, and the direct synthesis method was found to be the most well suited approach for obtaining a material with significant hydrothermal stability.

Regarding B-containing MCM-41, some work has been devoted to it in.<sup>10–15</sup> Trong *et al.*<sup>10</sup> used ludox and sodium silicate as a source of silica in a basic medium of TMAOH and NH<sub>4</sub>OH. The obtained B-MCM-41 possesses weak acidic strength compared to B-ZSM-5. Sundaramurthy *et al.*<sup>16</sup> prepared B-MCM-41 from ethylsilicate ester (silica source) and NaOH (basic source), the acidity reveals that the materials have only weak acidity and are lower than that of Al-MCM-41 and B-ZSM-5. Vaschetto *et al.*<sup>15</sup> analyzed the hydroxide source (NaOH and NH<sub>4</sub>OH) using tetraethoxysilane as silica source for B-MCM-41 synthesis. The adsorption of pyridine in sample followed by FT-IR, made it possible to identify a moderate Brønsted acidity due to the presence of hydroxyl groups.

Despite these works, the comparison of the acid sites between Al-MCM-41 and B-MCM-41 is not yet well determined. Dapurkar and Selvam<sup>17</sup> studied the acidity of the mesoporous material of Al-MCM-48 type. The analysis by temperature programmed desorption of ammonia made it possible to propose a model, which describe the nature of the acid sites into four types. In our study, the materials Si-, B-, Al- and B,Al-MCM-41 were synthesized by the direct method and using ludox (silica source), tetramethylammonium hydroxide (basic source) and sodium aluminate (source of aluminum). In order to make a comparison the nature of the acid sites between Si-, B-, Al- and B,Al-MCM-41, the adsorption of pyridine by FT-IR, allowed us to

assign the types of acid sites described by Dapurkar and Selvam to our materials.

## EXPERIMENTAL

### Synthesis

The synthesis procedures of Si-, B- and Al-MCM-41 have been reported in our previous publications.<sup>3,14,18,19</sup> All the hydrogels of the samples were prepared by the direct hydrothermal method, according to the following molar chemical composition: SiO<sub>2</sub>: 0.25CTAB: 0.2TMAOH: 0.08H<sub>3</sub>BO<sub>3</sub>: 0.04Al<sub>2</sub>O<sub>3</sub>: 40H<sub>2</sub>O.

*MCM-41 purely siliceous (Si-MCM-41)*: In an aqueous solution of TMAOH (tetramethyl ammonium hydroxide, TMAOH.5H<sub>2</sub>O, 25 wt.%, Aldrich), CTAB (C<sub>19</sub>H<sub>42</sub>NBr; Aldrich; 99%) was added. After 30 min of stirring, colloidal silica (ludox 40%, Prolabo) was subsequently added. The hydrogel was formed after 2 h of stirring.

*B-MCM-41 (Si/B = 12.5)*: The hydrogel preparation followed the same protocol as Si-MCM-41. Boric acid (H<sub>3</sub>BO<sub>3</sub>; Aldrich) was introduced after incorporating colloidal silica.

*Al-MCM-41 (Si/Al = 12.5)*: The hydrogel of this sample was formed by mixing three aqueous solutions, the first solution contains sodium aluminate, the second contains CTAB and the third contains colloidal silica. The first two solutions were added to the third one under vigorous stirring and the reaction mixture was continuously stirred for 2 h.

*B,Al-MCM-41 (Si/(B+Al) = 12.5)*: To achieve a ratio of 12.5, the amount in moles of boric acid was 0.04H<sub>3</sub>BO<sub>3</sub>, with B/Al = 1. The hydrogel formation process was identical to that of Al-MCM-41, with the exception that the boric source was added to the aqueous CTAB solution.

To transform the hydrogels into mesoporous materials, all samples were treated as follows: hydrothermal treatment at 100°C for 48 h; washing, filtration and drying overnight at 100°C and the as-synthesized samples were calcined at 550°C in air for 12 h.

### Characterization

To evaluate the structural and textural parameters of the mesoporous materials, the as-

synthesized and calcined samples were characterized by X-ray diffraction (Bruker D5005 diffractometer; Cu-K $\alpha$  radiation,  $\lambda = 1.5406 \text{ \AA}$ ; scanning step  $0.0358^\circ$  between  $1-10^\circ 2\theta$ ). N<sub>2</sub> physisorption at  $-196^\circ\text{C}$  (Nova 1000e; the samples were outgassed at  $200^\circ\text{C}$  for 24 h; the BET method<sup>20</sup> was used for specific surface area ( $S_{\text{BET}}$ ) determination; the pore size distribution ( $D_{\text{BJH}}$ ) was calculated using Barret-Joyner-Halenda formula), and Scanning Electron Microscopy (SEM) combined with an Energy Dispersive X-ray spectroscopy (EDX) (Philips ESEM XL 30 FEG). The nature and concentration of the acid sites of the various samples were evaluated by in situ pyridine adsorption / desorption FT-IR spectroscopy (Nicolet Avartar 360; a self-supporting wafer with 20 mg catalyst was placed into the in situ cell and was activated at  $200^\circ\text{C}$  for 4 h under 0.267 Pa. The sample was cooled to room temperature, and pyridine adsorption was performed in excess pure pyridine for 15 min followed by evacuation. FT-IR spectra was then recorded at room temperature of 50, 150, 250 and  $350^\circ\text{C}$  respectively. To determine the concentration of both types of acid sites, the extinction coefficients<sup>21</sup> used were  $\epsilon_{\text{B}} = 0.73 \text{ cm} \mu \text{ mol}^{-1}$  and  $\epsilon_{\text{L}} = 1.11 \text{ cm} \mu \text{ mol}^{-1}$ , for Brønsted and Lewis acid sites, respectively).

## RESULTS AND DISCUSSION

### Structural analysis

The XRD patterns of the as-synthesized and calcined Si-, B-, Al- or B,Al-MCM-41 materials are given in Fig. 1. The mesoporous MCM-41 material is characterized by a strong peak at  $2\theta = 2$  due to (100) reflection. The intensity of the peak varies after calcination depending on the incorporated heteroatom (aluminum and/or boron). The presence of diffraction peaks corresponding to (110), (200) and (210) reflections indicates the formation of well-ordered mesoporous materials.<sup>22</sup> The Si-MCM-41 (Fig. 1a), shows that after the calcination the intensity of the peaks corresponding to (100), (110), (200) and (210) reflections increase, this indicates a better structuring hexagonal channels of Si-MCM-41. The XRD analysis also shows

that the  $2\theta$  position is shifted to higher values, indicating a contraction of the unit cell parameter in the order of 9.8 % (Table 1). This phenomenon is caused by template removal and by condensation of the silanol groups.<sup>23</sup>

The analysis of B-MCM-41 by XRD pattern (Fig. 1b, Table 1), shows the same phenomena as Si-MCM-41. However, the contraction of the unit cell parameter is around 13.7% higher than that of Si-MCM-41 (9.8%). Valerio *et al.*<sup>24</sup> explained this difference by the presence of silanol groups ( $\equiv \text{SiOH}$ ), which is most important in the case of B-MCM-41 before calcination. By incorporating boron into the MCM-41 framework using boric acid ( $\text{H}_3\text{BO}_3$ ),  $\text{H}^+$  cations was also introduced. This latter will bond with the silicate anions ( $\equiv \text{SiO}^-$ ) to create silanol groups, thus the exchange of counterions of the template ( $\text{Br}^-$ ) by the silicate ions ( $\equiv \text{SiO}^-$ ) decreases, which reduces the spherical micelle/cylindrical micelle transition. For that the peak corresponding to (100) reflection of B-MCM-41 before calcination is less pronounced ( $I_{100} = 7197 \text{ u.a.}$ ), compared to as-synthesized Si-MCM-41 ( $I_{100} = 13647 \text{ u.a.}$ ).

The isomorphic substitution of the silicon atom by the aluminum atom ( $\text{Si/Al} = 12.5$ ) (Fig. 1c) or of both aluminum and boron atoms ( $\text{Si/(B+Al)} = 12.5$ ) (Fig. 1d), decreases the structural order of MCM-41, compared to purely silicic or boron incorporated materials. The disappearance of the peaks corresponding to (110) and (200) reflection which were observed in Si-MCM-41 and B-MCM-41 confirmed more disordered arrangement of channels for the Al-MCM-41 and B,Al-MCM-41. The incorporation of both heteroatoms, aluminum and boron with  $\text{Si/(B+Al)}$  ratio equal to 12.5 (Fig. 1d), causes other equidistant reflections to appear at  $2\theta = 3.4$  and  $6.8$ , these reflections characterize a lamellar phase MCM-50. The space between the layers of this phase must be filled with the template ( $\text{CTA}^+$ ), since the lamellar structure is destroyed after calcination. On the other hand, the peak corresponding to (100) reflection of the hexagonal phase becomes more intense ( $I_{100} = 1396 \text{ u.a.}$  before calcination to  $5901 \text{ u.a.}$  after calcination) (Table 1), this indicates that the hexagonal structure and the lamellar structure was not connected.<sup>25,26</sup> The calculated cell parameters are 41.60, 41.27, 43.94 and  $43.75 \text{ \AA}$  for Si-, B-, Al or B,Al-MCM-41 materials, respectively. In our previous work,<sup>14</sup> we explained that the substitution of elements into

MCM-41 material changes the T-O-T angle and T-O length (T = Si, B or Al). This confirms that the

heteroatoms were incorporated into the MCM-41 framework.

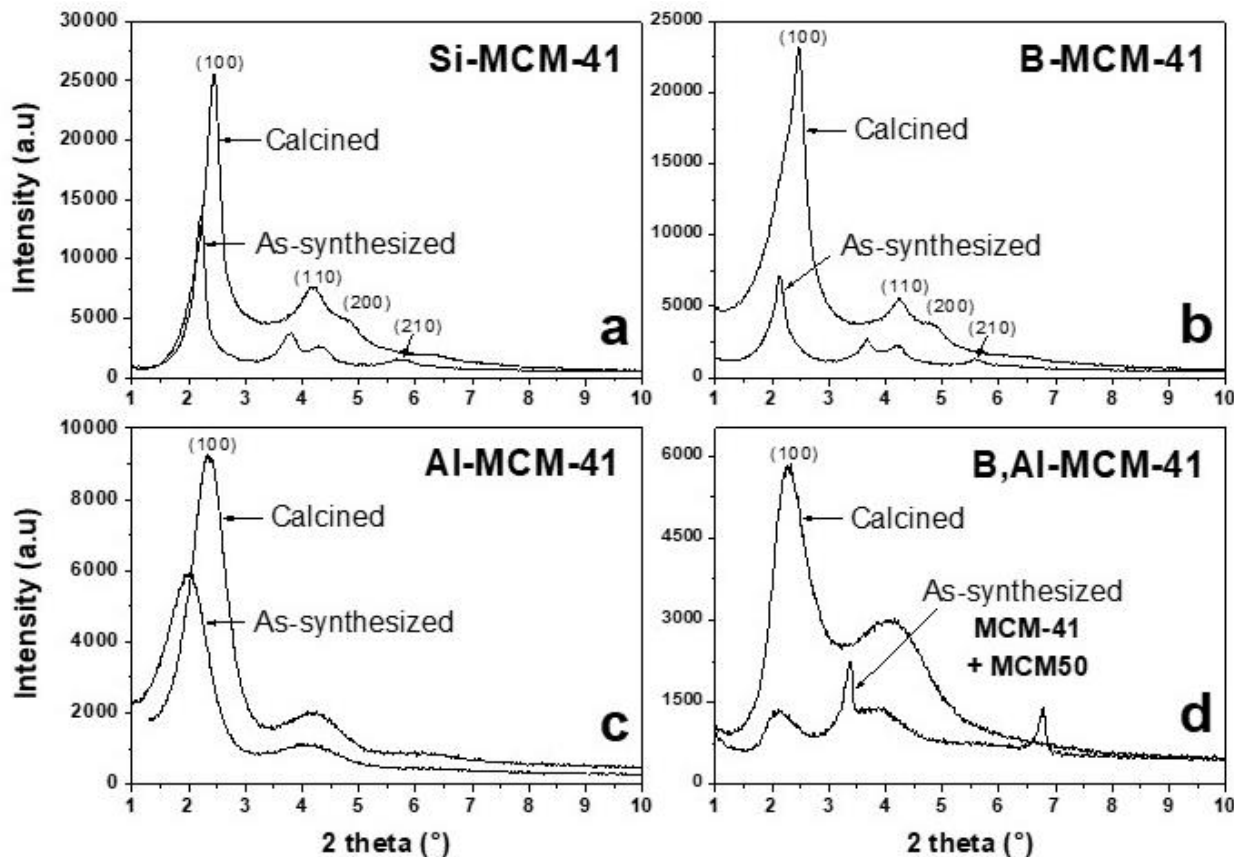


Fig. 1 – XRD patterns of as-synthesized and calcined Si-, B-, Al- or B, Al-MCM-41.

Table 1

XRD diffraction results

Sample	As-synthesized				Calcined				$\Delta a_0^d$ (%)
	$I_{100}^a$ (u. a)	2 theta (100)	$d_{100}^b$ (Å)	$a_0^c$ (Å)	$I_{100}$ (u. a)	2 theta (100)	$d_{100}$ (Å)	$a_0$ (Å)	
Si-MCM-41	13645	2.21	39.94	46.12	25718	2.45	36.03	41.60	9.8
B-MCM-41	7197	2.13	41.44	47.85	23310	2.47	35.74	41.27	13.7
Al-MCM-41	5994	2.04	43.27	49.96	9276	2.32	38.05	43.94	12.0
B,Al-MCM-41	1396	2.11	41.84	48.31	5901	2.33	37.89	43.75	9.4

<sup>a</sup> – Intensity of the reflection peak (100); <sup>b</sup> – XRD (100) interplanar spacing,  $n\lambda = 2d_{100} \sin\theta$ ; <sup>c</sup> – Unit cell determined for a hexagonal symmetry,  $a_0 = 2d_{100}/\sqrt{3}$ ; <sup>d</sup> –  $\Delta a_0$  (%) =  $([a_0(\text{as-synthesized}) - a_0(\text{calcined})] / a_0(\text{as-synthesized})) \times 100$ .

Figure 2 shows the N<sub>2</sub> physisorption isotherms and corresponding pore size distribution of the calcined Si-, B-, Al- or B, Al-MCM-41 and Table 2 summarizes their textural properties. All the

isotherms obtained are typical for MCM-41 structure. The corresponding isotherm is of type IV, characteristic of the mesoporous materials according to the IUPAC nomenclature.

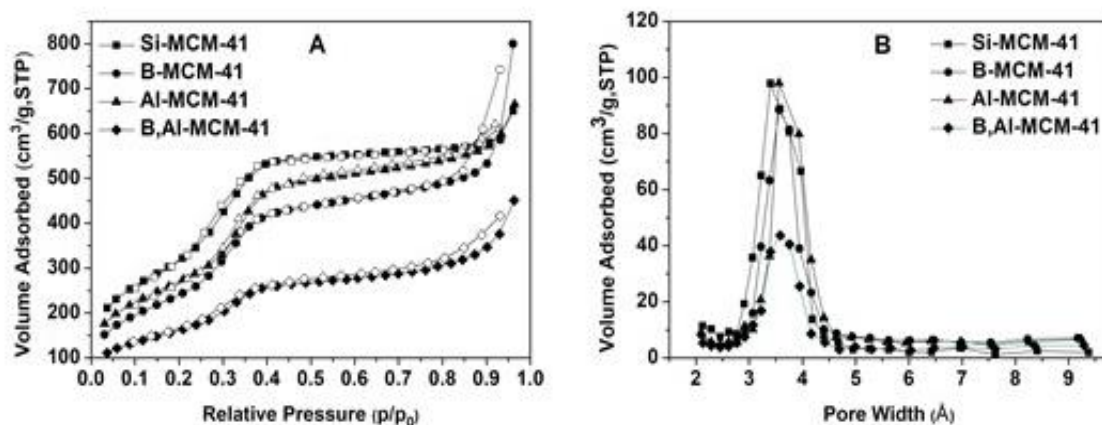


Fig. 2 – A) Nitrogen adsorption-desorption isotherms of calcined samples and B) BJH pore size distribution.

It is noted that the adsorption and desorption curves are practically merged, which predicts the uniformity of the mesopore size distribution. Indeed, the pore size distribution by the BJH method (Fig. 2B) confirms the homogeneous distribution of pore diameter. It is narrow and centered in the range of 34–36 Å (Table 2). The incorporation of heteroatoms into MCM-41 could change the textural properties of the material. The influence of this change was also observed in the N<sub>2</sub> physisorption for the calcined samples. The Si-MCM-41 showed a high  $S_{\text{BET}}$  (1154 m<sup>2</sup>g<sup>-1</sup>) and  $V_{\text{meso}}$  (0.84 cm<sup>3</sup>g<sup>-1</sup>). When the B, Al or B,Al were incorporated into MCM-41 framework, the  $S_{\text{BET}}$  and  $V_{\text{meso}}$  of the materials decreased in the

following order: Si-MCM-41 > Al-MCM-41 > B-MCM-41 > B,Al-MCM-41. In addition, the decrease in the unit cell ( $a_0 = 41.27$  Å) and wall thickness ( $W_t = 5.7$  Å) in presence of B compared to Si-MCM-41 ( $a_0 = 41.60$  Å,  $W_t = 7.6$  Å) confirms the incorporation of the boron in the MCM-41 framework. Contrary, in the presence of Al or B,Al, the  $a_0$  and  $W_t$  increases indicates that Al is incorporated into the framework, which was also observed in.<sup>27,28</sup> These variations should account for the differences in M-O bond distances (M = B<sup>3+</sup>, Si<sup>4+</sup> and Al<sup>3+</sup>): B-O (1.47 Å), Si-O (1.61 Å) and Al-O (1.76 Å).

Table 2  
Textural properties of the samples

Sample	2 theta (100)	$d_{100}$ (Å)	$a_0$ (Å)	$S_{\text{BET}}^a$ (m <sup>2</sup> g <sup>-1</sup> )	$V_{\text{meso}}^b$ (cm <sup>3</sup> g <sup>-1</sup> )	$D_{\text{BJH}}$ (Å)	$W_t^d$ (Å)
Si-MCM-41	2.45	36.03	41.60	1154	0.84	34.0	7.6
B-MCM-41	2.47	35.74	41.27	877	0.56	35.6	5.7
Al-MCM-41	2.32	38.05	43.94	983	0.76	35.6	8.4
B,Al-MCM-41	2.33	37.89	43.75	585	0.39	35.8	7.9

<sup>a</sup> Specific surface area; <sup>b</sup> Mesoporous volume; <sup>c</sup> Pore diameter determined by BJH; <sup>d</sup> Wall thickness =  $a_0 - D_p$ .

The morphology of the calcined solids was examined by scanning electron microscopy. SEM images and EDX graphs are shown in Fig. 3. Si-MCM-41 and B-MCM-41 have micellar rod-like-shaped hexagonal and particles which have no particular morphology. The images of Al-MCM-41 and B,Al-MCM-41 only show the presence of primary particles which have aggregated into

larger particles.<sup>15,29</sup> The EDX analysis confirms the incorporation of aluminum and/or boron atoms into the MCM-41 framework. These results agree with XRD and N<sub>2</sub> physisorption analysis. Thus, the structural and textural analyzes show that the solids containing heteroatoms retain the properties that characterize the mesoporous material of MCM-41 type.

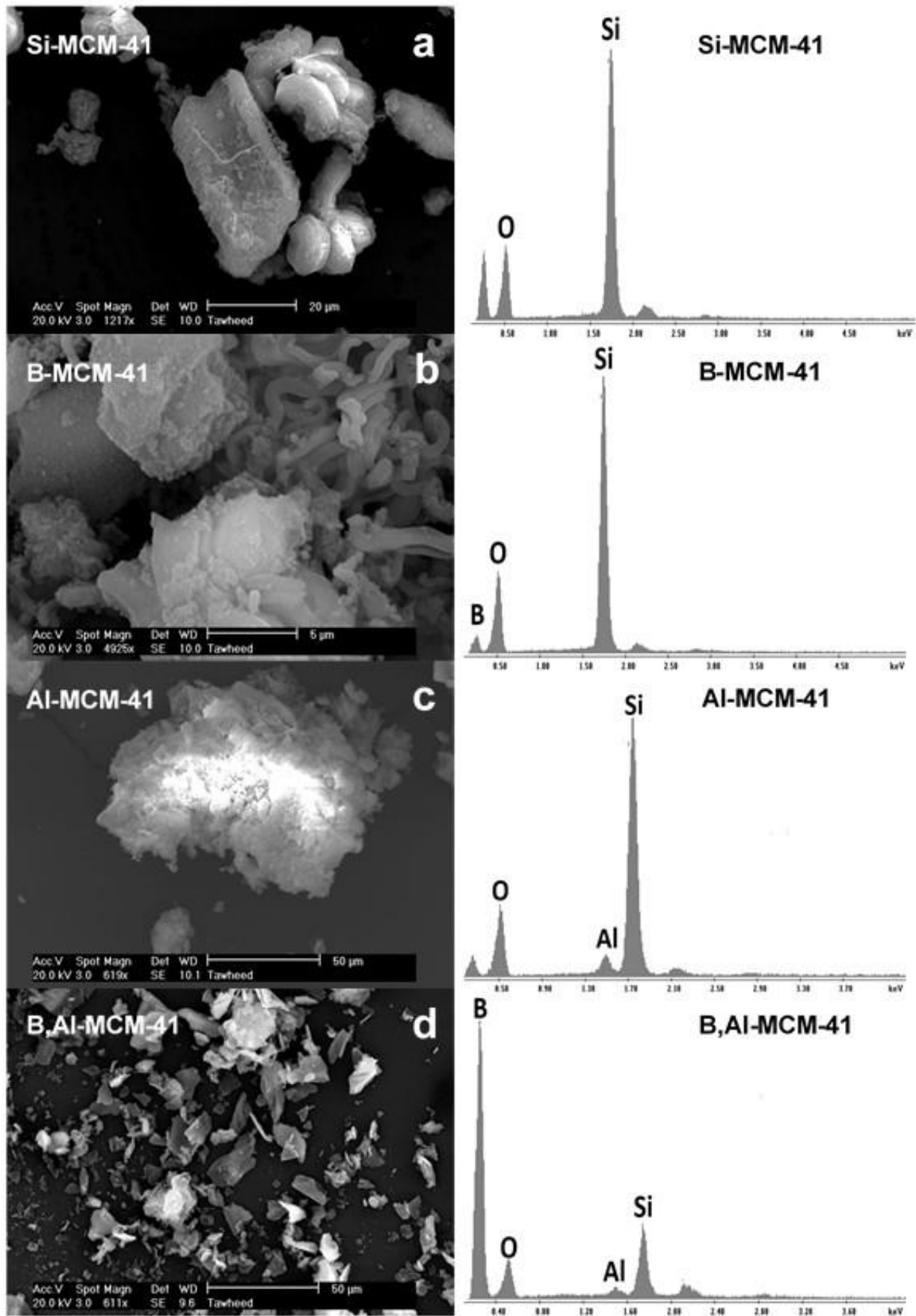
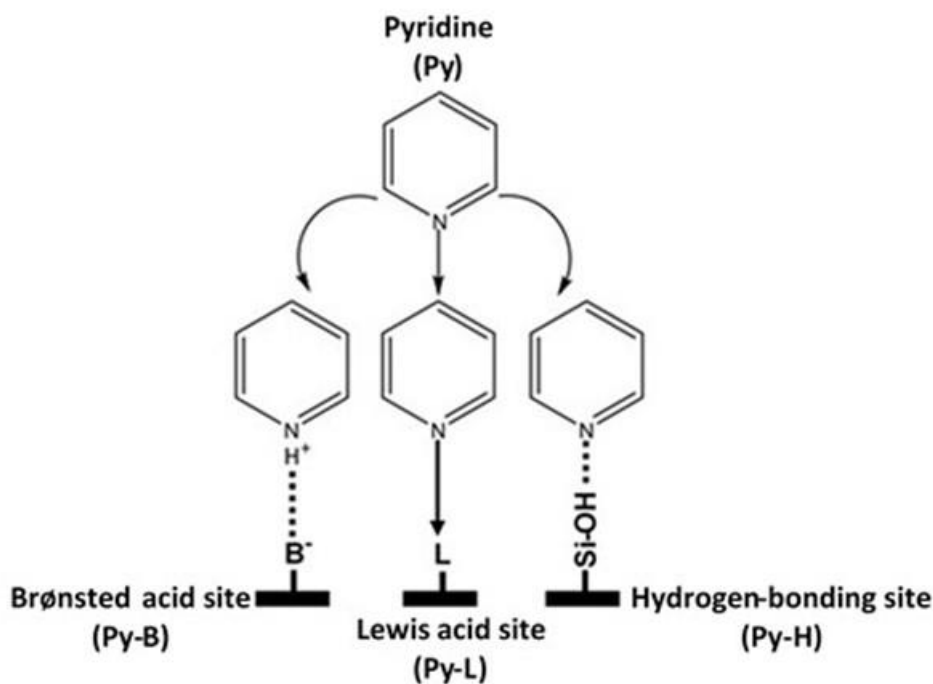


Fig. 3 – SEM and EDX of calcined samples.

### Spectroscopic analysis

The measurement of the acidity of MCM-41 was carried out by adsorption of a basic probe molecule followed by IR spectroscopy. Pyridine is a strong base ( $pK_b = 8.8$ ) commonly used in the case of zeolites and mesoporous materials. Its molecular diameter is 5.2 Å, which allows it to diffuse inside the porous volume of different

porous materials. The vibrations of the pyridine cycle adsorbed on the solid surface, show different bands between 1400 and 1650  $\text{cm}^{-1}$ . During its adsorption, pyridine protonates on the Brønsted sites (Py-B) (forming a pyridinium ion,  $\text{Py-H}^+$ ), coordinates with the Lewis sites (Py-L)<sup>30</sup> and can form hydrogen bonds with the silanol groups present in the structure<sup>30-33</sup> according to the Scheme 1.



Scheme 1 – Interactions between pyridine and acid sites.

Figure 4A shows the FT-IR spectra of pyridine adsorbed on Si-MCM-41, recorded after subsequent evacuation at 50, 150, 250, and 350°C. The spectra of the solid display bands at 1445 and 1596  $\text{cm}^{-1}$  assigned to silanol bonded pyridine (Py-H). These bands clearly decrease after evacuation at 250°C as expected for weak adsorption sites.

The spectrum of B-MCM-41 with Si/B ratio equal to 12.5 (Fig. 4B) presents the same bands as those of Si-MCM-41; these bands completely vanish after evacuation at 250°C. This sample also presents other bands at 1456 and 1622  $\text{cm}^{-1}$  which indicate the adsorption of pyridine on the Lewis acid sites. The very low intensity of these bands suggests a very weak Lewis acidity for this material.

FT-IR spectra of pyridine adsorbed on Al-MCM-41 (Si/Al = 12.5) and B,Al-MCM-41 (Si/(B+Al) = 12.5) are displayed in Figs. 4C and 4D, respectively.

The spectrum shows the same bands, which characterize the presence of the Brønsted and Lewis acid sites. The bands at 1456 and 1622  $\text{cm}^{-1}$  indicate the adsorption of pyridine on Lewis acid sites while bands at 1545 and 1635  $\text{cm}^{-1}$  indicate adsorption of pyridine on Brønsted acid sites. The band at 1490  $\text{cm}^{-1}$  assigned to pyridine associated with both Brønsted and Lewis acid sites. Their intensity persists when the outgassing temperature increases. This shows that these solids have a stable acidity of the Brønsted and Lewis even upon outgassing at 350°C. At 50°C (Figs. 4Ca and 4Da), Al-MCM-41 and B,Al-MCM-41 also show the characteristic bands of Py-H (1445 and 1596  $\text{cm}^{-1}$ ) previously observed for the purely siliceous MCM-41 and Boron containing MCM-41. Marques *et al.*<sup>34</sup> and Lourenço *et al.*<sup>35</sup> also observed this. A pyridine molecule can be adsorbed on a Lewis acid site and interacting through hydrogen bonding with a proton site.

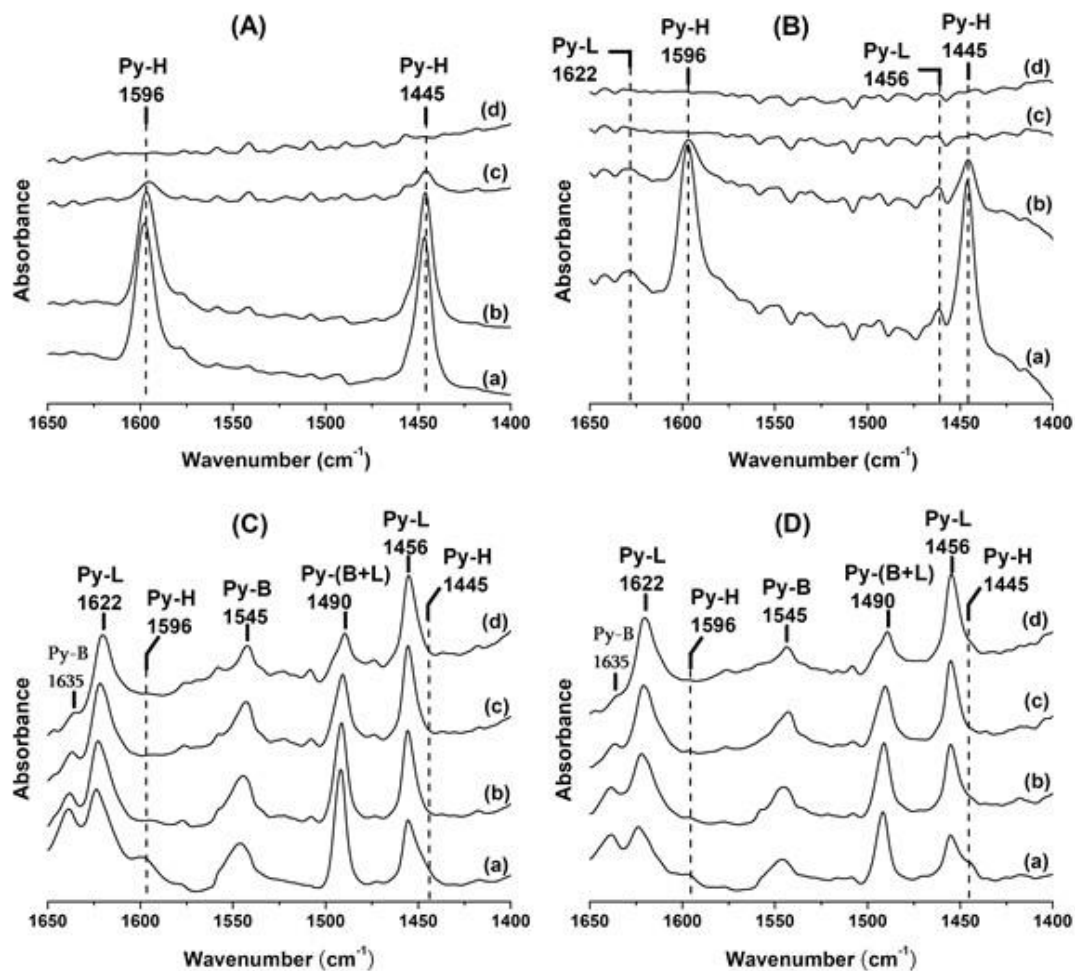


Fig. 4 – FT-IR spectra of pyridine desorbed on calcined samples under vacuum 3 Torr pressure at: a) 50°C; b) 150°C; c) 250°C; d) 350°C. A) Si-MCM-41; B) B-MCM-41; C) Al-MCM-41; D) B,Al-MCM-41.

For Al-MCM-41 (Fig. 5a), the concentration of the Lewis acid sites remains stable, whereas the Brønsted decreases with increasing outgassing temperature. The

concentration of the Lewis acid sites of B,Al-MCM-41 (Fig. 5b), remains stable up to 350°C, while whereas the Brønsted remains stable up to 250°C.

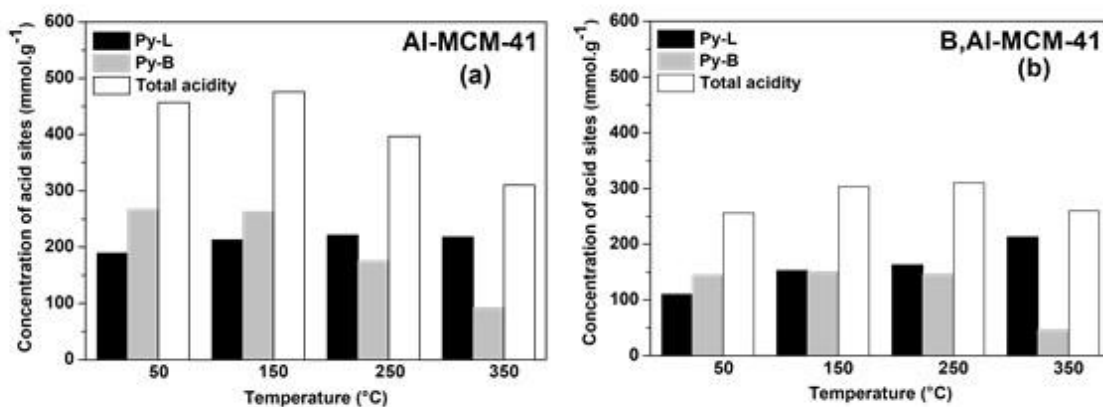


Fig. 5 – Brønsted ( $C_B$ ) and Lewis ( $C_L$ ) acidity of calcined samples measured by FT-IR spectroscopy combined with pyridine adsorption and desorption at different temperatures: a) Al-MCM-41; b) B,Al-MCM-41

The  $C_L/C_B$  ratio of Al-MCM-41 (Fig. 6) shows that this sample has Brønsted acid sites up to 150°C. At 250 and 350°C, Lewis acid sites becomes predominant. For B,Al-MCM-41 at 50°C, the  $C_L/C_B$  ratio gives priority to Brønsted acid sites. Above

this temperature, Lewis acid sites predominate. The presence of the Brønsted and Lewis acid sites in B,Al-MCM-41 is due only to the incorporation of aluminum atoms into the framework of the mesoporous material.

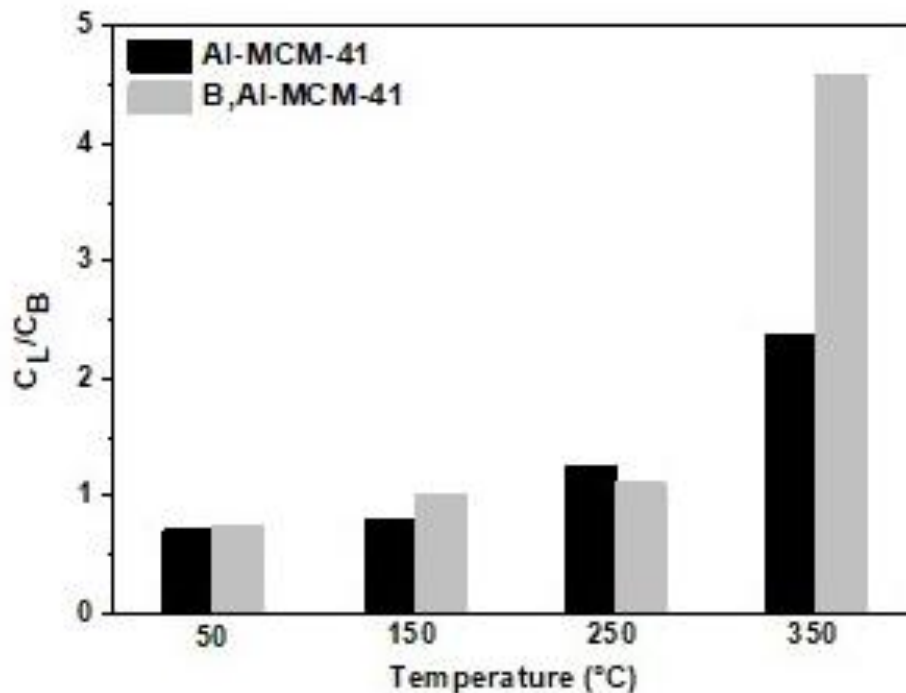


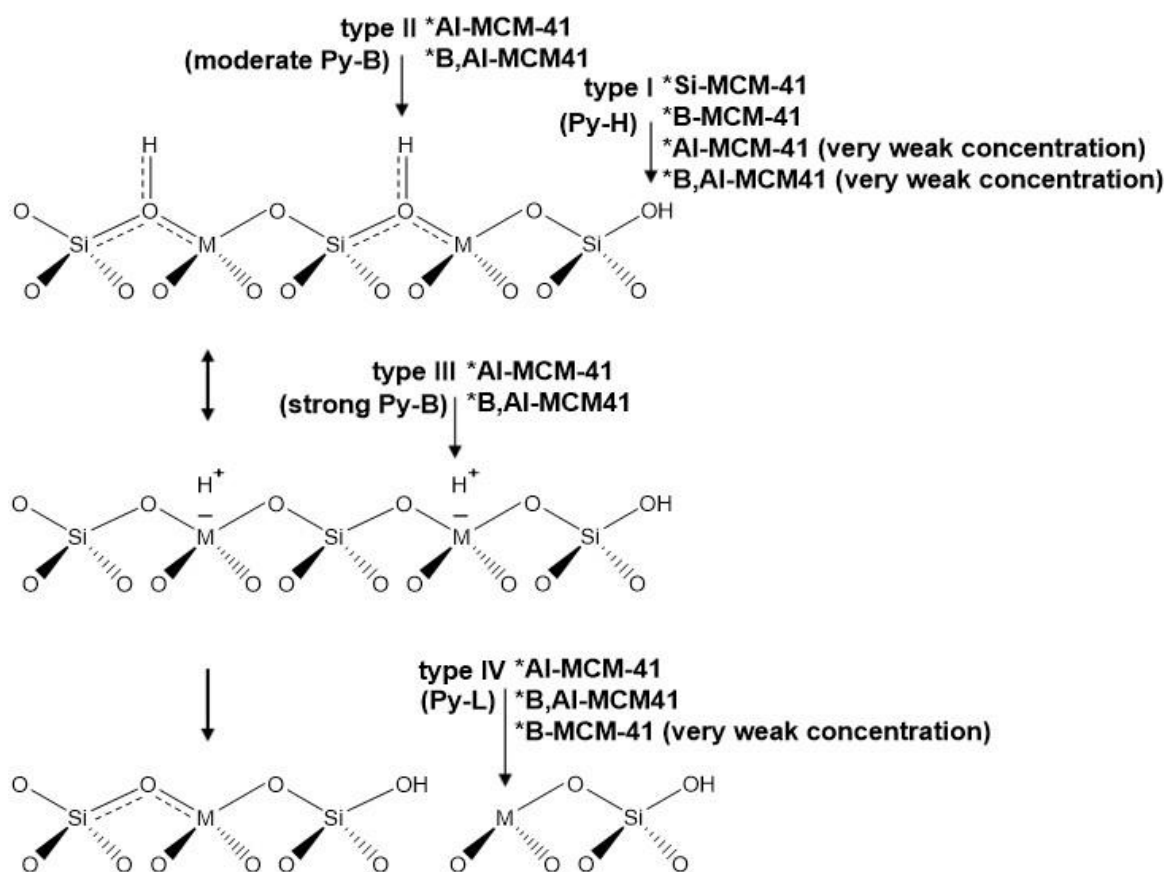
Fig. 6 –  $C_L/C_B$  ratio of Al-MCM-41 and B,Al-MCM-41.

We previously explained that the presence of the boron atom affects the structure and texture of the MCM-41 (XRD,  $N_2$  physisorption) favoring the formation of silanol groups. These have been confirmed by FT-IR spectra of pyridine adsorbed on B-MCM-41. For that, the presence of boron atoms reduced the total acidity in B,Al-MCM-41 compared with Al-MCM-41 (Fig. 5).

Dapurkar and Selvam<sup>17</sup> have described the nature of the acid sites of H-Al-MCM-48. From the characterization results, they proposed four types of acid sites: type (I) is due to surface hydroxyl groups from weak acid sites (hydrogen-bonding site (Py-H)). Type (II) and type (III) originate from moderate and strong Brønsted acid sites (Py-B) that are due to the presence of metal element in two different framework positions and type (IV) is attributed to Lewis acid sites. A schematic representation of nature of the acid sites of our Si-, B-, Al- or B,Al-MCM-41 materials is shown in scheme 2. The nature of the

acid sites of Si- and B-MCM-41 are of type I (Py-H). B-MCM-41 has also type IV (Py-L) of very weak concentration. Al- and B,Al-MCM-41 are characterized by acid sites type II/III (Py-B), type IV (Py-L) and type I (Py-H) of very weak concentration.

The acidic nature of MCM-41 (types hydrogen-bonding (I), Brønsted (II)/(III), or Lewis (IV)) governs their catalytic performance. Si-MCM-41, with very low acidity (type I), acts as a support for mild reactions (aldol, Knoevenagel).<sup>36</sup> B-MCM-41, with weak hydrogen-bonding sites (type I) and Lewis sites (type IV), is active in oxidative dehydrogenation.<sup>37</sup> Al-MCM-41 exhibits a high density of Brønsted (type III) and Lewis (type IV) sites, active in cracking, isomerization, and transesterification.<sup>38–40</sup> Recent catalytic performances show that adapting the type of active site to the process is essential. Thus, each doping determines a unique acid profile, and therefore a specific application.



Scheme 2 – Representation of nature of the acid sites in Si-, B-, Al- and B,Al-MCM-41 materials (adapted from<sup>17</sup>).

## CONCLUSIONS

Boron and/or aluminum incorporated in the mesoporous MCM-41 material were prepared by the direct hydrothermal synthesis method. The structural and textural analyzes carried out by XRD, N<sub>2</sub> physisorption and SEM/EDX confirmed the incorporation of boron and aluminum atoms in MCM-41 framework.

The spectroscopic analysis of the adsorption of pyridine on the materials after desorption at different temperatures, revealed that the nature of the acid sites of B-MCM-41 is of type I (Py-H), which is the same as that of Si-MCM-41. Additionally, there is the presence of type IV (Py-L) at very low concentration. Al-MCM-41 and B,Al-MCM-41 have acid sites type II/III (Py-B), type IV (Py-L) and type I (Py-H) of very low concentration.

## REFERENCES

1. A. Corma, A. Martínez, V. Martínez-Soria and J. B. Montón, *J. Catal.*, **1995**, *153*, 25–31.
2. A. Sayari, *Chem. Mater.*, **1996**, *8*, 1840–1852.
3. L. Brahmi, T. Ali-Dahmane, R. Hamacha and S. Hacini, *J. Mol. Catal. A Chem.*, **2016**, *423*, 31–40.
4. Y. Doussaid, T. Ali-Dahmane, N. Mehiaoui, L. Brahmi, Z. Kibou, R. Hamacha and N. Choukchou-Braham, *Lett. Org. Chem.*, **2021**, *18*, 1–6.
5. P. J. Branton, P. G. Hall and K. S. W. Sing, *J. Chem. Soc. Chem. Commun.*, **1993**, 1257–1258.
6. J. Rathousky, A. Zukai, O. Franke and G. Schulz-Ekloff, *J. Chem. Soc. Faraday Trans.*, **1994**, *90*, 2821–2826.
7. J. S. Beck, J. C. Vartuli, W. J. Roth, M. E. Leonowicz, C. T. Kresge, K. D. Schmitt, C. T. W. Chu, D. H. Olson, E. W. Sheppard, S. B. McCullen, J. B. Higgins and J. L. Schlenkert, *J. Am. Chem. Soc.*, **1992**, *114*, 10834–10843.
8. C. T. Kresge, M. E. Leonowicz, W. J. Roth, J. C. Vartuli and J. S. Beck, *Nature*, **1992**, *359*, 710–712.
9. R. B. Borade and A. Clearfield, *Catal. Lett.*, **1995**, *31*, 267–272.
10. D. Trong On, P. N. Joshi, J. Lemay and S. Kaliaguine, *Surf. Sci. Catal.*, **1995**, *97*, 543–549.
11. A. Sayari, C. Danumah and I. L. Moudrakovski, *Chem. Mater.*, **1995**, *7*, 813–815.
12. A. Chenite, Y. Le Page and A. Sayari, *Chem. Mater.*, **1995**, *7*, 1015–1019.
13. U. Oberhagemann, I. Topalovic, B. Marler and H. Gies, *Stud. Surf. Sci. Catal.*, **1995**, *98*, 17–18.
14. M. Adjdir, T. Ali-Dahmane and P. G. Weidler, *C. R. Chim.*, **2009**, *12*, 793–800.
15. E. G. Vaschetto, G. A. Pecchi, S. G. Casuscelli and D. A. Eimer, *Microporous Mesoporous Mater.*, **2016**, *258*, 269–276.
16. V. Sundaramurthy and N. Lingappan, *Microporous Mesoporous Mater.*, **2003**, *65*, 243–255.

17. S. E. Dapurkar and P. Selvam, *Appl. Catal. A Gen.*, **2003**, *254*, 239–249.
18. T. Ali-Dahmane, L. Brahmī, R. Hamacha, S. Hacini and A. Bengueddach, *Bull. Chem. React. Eng.*, **2019**, *14*, 358–368.
19. T. Ali-Dahmane, L. Brahmī, R. Hamacha and A. Bengueddach, *Ann. Chim. Sci. Mat.*, **2017**, *40*, 149–163.
20. S. Brunauer, P. H. Emmett and E. J. Teller, *J. Am. Chem. Soc.*, **1938**, *60*, 309–319.
21. J. Dakta, A. M. Turek, J. M. Jehng and I. E. Wachs, *J. Catal.*, **1992**, *135*, 186–199.
22. T. R. Pauly, Y. Liu, T. J. Pinnavaia, S. J. L. Billinge and T. P. Rieker, *J. Am. Chem. Soc.*, **1999**, *121*, 8835–8842.
23. K. J. Edler and J. W. White, *Chem. Mater.*, **1997**, *9*, 1226–1233.
24. G. Valerio, J. Plevert, A. Goursot and F. di Renzo, *Phys. Chem. Chem. Phys.*, **2000**, *2*, 1091–1092.
25. M. Busio, J. Janchen and J. H. C. van Hooff, *Microporous Mater.*, **1995**, *5*, 211–218.
26. J. L. Blin, C. Otjacques, G. Herrier and B. L. Su, *Int. J. Inorg. Mater.*, **2001**, *3*, 75–86.
27. S. Liu, H. He, Z. Luan and J. Klinowski, *J. Chem. Soc. Faraday Trans.*, **2015**, *92*, 2011–2015.
28. V. Sundaramurthy, I. Eswaramoorthi and N. Lingappan, *Can. J. Chem.*, **2004**, *82*, 631–640.
29. M. A. Betiha, S. A. Mahmoud, M. F. Menoufy and A. M. Al-Sabagh, *Appl. Catal. B*, **2011**, *107*, 316–326.
30. T. Yamamoto, T. Tanaka, T. Funabiki and S. Yoshida, *J. Phys. Chem. B*, **1998**, *102*, 5830–5839.
31. A. Jentys, K. Kleestorfer and H. Vinek, *Microporous Mesoporous Mater.*, **1999**, *27*, 321–328.
32. T. D. Conesa, J. M. Hidalgo, R. Luque, J. M. Campelo and A. A. Romero, *Appl. Catal. A: Gen.*, **2006**, *299*, 224–234.
33. E. G. Vaschetto, G. A. Monti, E. R. Herrero, S. G. Casuscelli and G. A. Eimer, *Appl. Catal. A: Gen.*, **2013**, *453*, 391–402.
34. J. P. Marques, I. Gener, P. Ayrault, J. C. Bordado, J. M. Lopes, F. R. Ribeiro and M. Guisnet, *Microporous Mesoporous Mater.*, **2003**, *60*, 251–262.
35. J. P. Lourenço, A. Fernandes, C. Henriques and M. F. Ribeiro, *Microporous Mesoporous Mater.*, **2006**, *94*, 56–65.
36. K. Snigdha, T. N. M. Musthafa, A. M. Asiri, K. A. Alamry and M. Assad, *Journal of Molecular Modeling*, **2023**, *29*, 244.
37. Q. Liu, J. Wang, Z. Liu, R. Zhao, A. Xu, and M. Jia, *ACS Omega*, **2022**, *7*, 3083–3092.
38. Y. Xiong, Y. Jia, Y. Du, X. Du, X. Feng, W. Shan and H. Yu, *Fuel*, **2025**, *386*, 134265.
39. V. V. Zamalyutin, E. V. Okuneva, S. S. Moskvichev, *Catal. Ind.*, **2025**, *17*, 133–156.
40. M. Anwar, M. E. Konnova and S. Dastgir, *RSC Sustainability*, **2025**.

